

Probing hadronic formation times with antiprotons in $p + A$ reactions at AGS energies *

W. Cassing¹, E. L. Bratkovskaya², O. Hansen³

¹Institut für Theoretische Physik, Universität Giessen
D-35392 Giessen, Germany

²Institut für Theoretische Physik, Universität Frankfurt
D-60054 Frankfurt, Germany

³Niels Bohr Institute, University of Copenhagen
2100 Copenhagen, Denmark

November 3, 2018

Abstract

The production of antiprotons in $p + A$ reactions is calculated in a microscopic transport approach employing hadronic and string degrees of freedom (HSD). It is found that the abundancies of antiprotons as observed by the E910 Collaboration in $p + A$ reactions at 12.3 GeV/c as well as 17.5 GeV/c can approximately be described on the basis of primary proton-nucleon and secondary meson-baryon production channels for all targets. The transport calculations demonstrate that the antiproton rapidity distributions for heavy targets are sensitive to the \bar{p} (or hadron) formation time in the nuclear medium. Within our analysis the data from the E910 Collaboration are reasonably described with a formation time of 0.4 – 0.8 fm/c in the hadron rest frame.

PACS: 24.10.-i; 24.10.Cn; 24.10.Jv;

Keywords: Nuclear reaction models and methods; Many-body theory; Relativistic models;

*Supported by the European Graduate School 'Complex Systems of Hadrons and Nuclei', Copenhagen-Giessen

1 Introduction

Since the first observation of antiproton production in proton-nucleus [1, 2, 3] and nucleus-nucleus collisions [4, 5, 6] the production mechanism has been quite a matter of debate. Especially in nucleus-nucleus collisions at subthreshold energies traditional cascade calculations, that employ free NN production and $\bar{p}N$ annihilation cross sections, essentially fail in describing the high cross sections seen from 1.5 - 2.1 A-GeV [7, 8]. Thus multiparticle nucleon interactions [9, 10] have been suggested as a possible solution to this problem. On the other hand it has been pointed out that the quasi-particle properties of the nucleons and antinucleons might be important for the \bar{p} production process which become more significant with increasing nuclear density [11, 12, 13, 14, 15, 16]. Relativistic transport calculations have indicated that all the low energy data from proton-nucleus and nucleus-nucleus collisions are compatible with attractive \bar{p} self energies (at normal nuclear matter density ρ_0) in the order of -100 to -150 MeV [16, 17, 18]. However, it had been stressed at that time that the high antiproton yield might also be attributed to mesonic production channels [19] since $p\bar{p}$ annihilation leads to multi-pion final states with an average abundancy of 5 pions [20].

With new data coming up on antibaryon production from proton-nucleus and nucleus-nucleus collisions at the AGS [21, 22, 23, 24, 25] and SPS [26, 27, 28, 29] the $\bar{p}, \bar{\Lambda}$ enhancement factors seen experimentally were no longer that dramatic as at SIS energies, however, traditional cascade calculations employing free production and annihilation cross sections again were not able to reproduce the measured abundancies and spectra [30, 31, 32, 33] especially for $\Xi, \bar{\Xi}$ and $\Omega, \bar{\Omega}$. Here additional collective mechanisms in the entrance channel have been suggested such as color rope formation [34] or hot plasma droplet formation [35]. In another language this has been addressed also as string fusion [36, 37], a precursor phenomenon for the formation of a quark-gluon plasma (QGP).

The intimate connection of antibaryon abundancies with the possible observation of a new state of the strongly interacting hadronic matter, i.e. the quark-gluon plasma, has been often discussed since the early suggestion in Ref. [38] that especially the enhanced yield of strange antibaryons – approximately in chemical equilibrium with the other hadronic states – should be a reliable indicator for a new state of matter. In fact, the data on strange baryon and antibaryon production from the NA49 and WA97 Collaborations show an approximate chemical equilibrium [39, 40, 41] with an enhancement of the Ω^-, Ω^+ yield in central $Pb + Pb$ collisions (per participant) relative to pBe collisions at the same invariant energy per nucleon by a factor ~ 15 . As pointed out in Ref. [42] the data on multi-strange antibaryons at the SPS seem compatible with a canonical ensemble in chemical equilibrium.

In Ref. [43] Rapp and Shuryak have proposed multi-meson production channels for $p\bar{p}$ pairs to describe the antiproton abundancies in central $Pb + Pb$ collisions at the SPS. Later on, Greiner and Leupold [44] have applied the same concept for the $\bar{\Lambda}$ production by a couple of mesons including a K^+ or K^0 (for the \bar{s} quark). In fact, their estimates have been supported by the microscopic multi-particle calculations in Ref. [45] employing detailed balance relations for 2 hadron \leftrightarrow n hadron transi-

tions and vice versa. Thus, in case of relativistic nucleus-nucleus collisions at AGS and SPS energies the low effective antibaryon absorption seen experimentally can naturally be explained by the backward reaction channels, i.e. multi-meson fusion channels.

The latter mechanism, however, does not apply to proton-nucleus reactions since there is no longer an approximately thermal 'meson bath' feeding the baryon-antibaryon production channel as pointed out in Ref. [45]. Nevertheless, the \bar{p} yield measured by the E910 Collaboration in $p + A$ reactions at 12.3 GeV/c and 17.5 GeV/c was found to be surprisingly high [25]. An analysis within the Glauber model showed that either the annihilation cross section σ_{ann} should be small compared to the cross section in free space or the \bar{p} formation time τ_F should be a couple of fm/c when employing the free annihilation cross section [25]. The authors of the latter work conclude that the 'naive' first-collision model with subsequent annihilation of antiprotons is incompatible with their data supporting the earlier finding from Ref. [46], where previous data from $p + A$ and $A + A$ reactions had been analysed within a similar model.

In this work we will address \bar{p} production in proton-nucleus collisions at 12.3 GeV/c and 17.5 GeV/c within the covariant HSD¹ transport approach [47] which is based on the concept of string formation and decay at invariant collision energies $\sqrt{s} \geq 2.6$ GeV for baryon-baryon collisions and $\sqrt{s} \geq 2.3$ GeV for meson-baryon collisions, while the low-energy reactions are described by known vacuum cross sections or resonance formation and decay cross sections. A single sensitive parameter in this approach is the string duration or hadron formation time $\tau_F \approx 0.7\text{-}0.8$ fm/c which has been fitted to the proton rapidity distribution in nucleus-nucleus collisions at SPS energies [47] and kept fixed furtheron. For more details we refer the reader to the review [17].

2 Qualitative considerations

The physical picture within this transport approach for \bar{p} production in $p + A$ reactions is as follows: The impinging proton might create a $N\bar{N}$ pair in a first collision at position x_1 (cf. Fig. 1) and the prehadronic quark-antiquark configuration travels essentially in forward direction by a time $\gamma\tau_F$ – where γ denotes the Lorentz dilatation factor – until the hadronic \bar{p} emerges at position x_2 . The hadronic state then propagates further in the same direction and reacts with the remaining nucleons elastically or inelastically. In the latter phase the dominant channel will be annihilation with a cross section

$$\sigma_{ann}(\sqrt{s}) = \frac{50[mb]}{v_{rel}}, \quad (1)$$

where the relativistic relative velocity is given by [48]

$$v_{rel} = \frac{\sqrt{(s - M_1^2 - M_2^2)^2 - 4M_1^2 M_2^2}}{2E_1 E_2}, \quad (2)$$

¹Hadron-String-Dynamics

which is evaluated in the lab. frame. As shown in Fig. 3 of Ref. [45] the expression (1) well describes the experimental data [49, 50] on \bar{p} annihilation for relative momenta up to 2–3 GeV/c.

In rapidity space the produced antibaryons will be localized around midrapidity y_m ; fast antiprotons hadronize later than slow \bar{p} 's due to the larger γ factor and in view of (1) also experience a smaller annihilation cross section. Thus antiprotons from first-chance collisions in heavy nuclei should result in rapidity distributions that are highly asymmetric with respect to midrapidity and a larger suppression should be observed for $y \leq y_m$ than for $y \geq y_m$, if the target is located at $y = 0$. In fact, a simple look at the experimental \bar{p} rapidity distribution from Fig. 2 of Ref. [25] does not support the first-collision picture.

On the other hand, in Ref. [16] it was found that a dominant fraction of antiprotons emerge from secondary pion-nucleon reactions in $p + A$ reactions at lower energies. Such secondary reaction channels might also be a reason for the observations of Ref. [25] since the \bar{p} production cross section in πN reactions close to threshold is large compared to the production cross section in pp collisions (cf. Fig. 6 of Ref. [16]). The dynamical effects of such secondary production channels are easy to map out within the string/hadron dynamical picture: In a first pN collision a 'meson' ($q\bar{q}$ pair) M is produced at position x_1 which hadronizes after time $\gamma_M \tau_F$ at position x_2 . Then it propagates on average for a distance $\lambda_M \sim (\sigma_{tot} \rho_0)^{-1} \approx 2$ fm (in the lab. frame of reference) before reacting with another nucleon. In this reaction (at position x_3) it may also produce a pre- $N\bar{N}$ pair which hadronizes after time $\gamma \tau_F$ in position x_4 . Then the antinucleon propagates in the same direction and may be rescattered, annihilated or emerge to free space. The antibaryons from secondary – or even ternary – processes have a much shorter way to escape the nucleus without being annihilated than those from first-chance collisions. Furthermore, their initial rapidity distribution will be shifted closer to target rapidity because the primary mesons are produced symmetrically around y_m and only the energetic mesons will give a sizeable contribution to the \bar{p} production provided that they hadronize in the medium.

As mentioned above we here adopt the HSD transport approach that has e.g. been tested in Ref. [51] for pion production and proton stopping in $p + A$ reactions at AGS energies using $\tau_F = 0.8$ fm/c. Since the description of the related data is very satisfactory (cf. Fig. 8 in Ref. [51]) we continue with aspects of meson formation and secondary interactions, that are relevant for antiproton production and propagation in $p + A$ reactions.

In order to achieve a quantitative idea about the time scales for meson production and propagation we show in Fig. 2 for $p + Au$ at 12.3 GeV/c the time dependence of the 'formed' meson number (solid line) in comparison to the number of string-like $q\bar{q}$ excitations (dashed line) that convert to mesons on a time scale of τ_F in their individual rest frame. The reference frame for the transport calculation is the nucleon-nucleon cms. (at $y_{lab} \approx 1.63$) with a Lorentz γ -factor of ≈ 2.67 for the projectile proton and target nucleus, respectively, such that the dimensions of the target in space - as seen by the hadrons - are squeezed by the factor γ . The sharp increase of the dashed line at $t=0$ denotes the beginning of the $p + Au$ reaction

with the excitation of strings that may lead to the formation of $N\bar{N}$ pairs, too. The latter also appear as hadronic states on a similar time scale as the mesons – approximately 2 fm/c later – and may be annihilated or rescattered on the residual target nucleons. We recall that only the formed hadronic states are allowed to interact with the nucleons of the target again and to produce secondary mesons or baryon-antibaryon pairs. Thus antiprotons or mesons, that move fast with respect to the target at rest, may only form in the vacuum and not interact in the nucleus again. In fact, this is approximately the case for a Be -target at this energy, while the dominant fraction of hadrons are formed inside the Au -nucleus and reinteract again (see below). For completeness we note, that the increase of the meson number for $t \geq 7$ fm/c is essentially due to the decays of mesonic resonances (ρ, ω, ϕ, K^*) that increase the net meson number.

The distribution in the invariant collision energy \sqrt{s} is shown in Fig. 3 for $p + Au$ at 12.3 GeV/c for baryon-baryon (BB) collisions (solid line) in comparison to the reactions of formed mesons with nucleons (mB , dashed line). The high energy peak of the BB -distribution (around $\sqrt{s} \approx 5$ GeV) is due to primary pN collisions; it is smeared out substantially due to Fermi motion. The low energy peak of the BB -distribution reflects multiple scattering of baryons in the target that, however, do not contribute to $p\bar{p}$ production due to the threshold of ~ 3.75 GeV (solid arrow). The \sqrt{s} distribution for interactions of formed mesons with baryons (dashed line) extends to about 4.5 GeV, which is well above the $\bar{p}p$ production threshold of ~ 2.8 GeV (dashed arrow). The distribution in the collision number above threshold is substantially larger for BB -reactions than for meson-nucleon collisions, however, the distributions have to be 'folded' with the respective $p\bar{p}$ production cross sections. We recall that in πN reactions close to threshold this cross section is large compared to the production cross section in pp collisions (cf. Fig. 6 of Ref. [16]) such that the mB channels might well compete with the BB channels.

3 Comparison to data

It should be noted that for the present analysis the perturbative production scheme of Ref. [16] has been employed due to the low multiplicities for \bar{p} production ($\sim 2 \times 10^{-4}$ for $p + Au$ at 12.3 GeV/c). All cross sections are the same as in the latter work; the only modification introduced is a new parametrisation of the individual rapidity (y) and transverse momentum (p_T) dependence for antiprotons in the elementary pN and πN production channels, since the kinematical regime is substantially different from the latter study and the final states can no longer be described accurately by 4- or 3-body phase-space, respectively. To this aim high statistics event generation has been performed within the LUND string model [52] – as implemented in the HSD approach – for \bar{p} production and the resulting two-dimensional spectra have been fitted by a Gaussian in rapidity and exponential in $p_T^2(y)$. As demonstrated in Refs. [17, 51] the LUND model works rather well for this purpose in comparison to the available data [50], however, uncertainties in the order of 50% for the elementary cross sections cannot be ruled so far since there are no data available for invariant

energies close to threshold.

With the input cross sections defined we can step on with a quantification of the physics addressed above. In Fig. 4 we show the \bar{p} rapidity spectra for $p + Be$ at 12.3 GeV/c in comparison to the experimental data from [25]. The dashed line ($BB_{prim.}$, upper part) gives the \bar{p} spectrum from BB production channels prior to final state interactions (FSI). The contribution from secondary mB collisions is not visible on a linear scale for the Be target. When including \bar{p} rescattering as well as annihilation the dash-dotted line (BB_{final}) is obtained for BB production channels. It is clearly seen that \bar{p} annihilation is more pronounced for low rapidities – with the target at $y = 0$ – than for $y \geq y_m \approx 1.63$. Thus for $p + Be$ the pN production channel clearly dominates and the comparison with the experimental rapidity distribution (lower part of Fig. 4) essentially tests the adequacy of the elementary differential \bar{p} production cross section in pN collisions which appears to be underestimated slightly (by about 30%) in the present approach using the input from Ref. [16] and assuming that the data point for $y = 1.1$ is solid. One might rescale the elementary cross section accordingly, however, the focus of our present work is not on fitting data. On the other hand, antiprotons from a feeddown of $\bar{\Lambda}$ and $\bar{\Sigma}^0$ might also be contained in the data while they are excluded in the calculation². Thus, provided that the reactions are described properly in the HSD transport approach, the cross sections for all targets should be low by about 30%, too, in case the \bar{p} yield is dominated by the BB channels (see below).

The numerical results for $p + Cu$ and $p + Au$ at 12.3 GeV/c are shown in Figs. 5 and 6 adopting the same assignment of the lines as in Fig. 4. It is clearly seen that for the Cu -target the contribution from mB collisions – as displayed by the short dashed line ($mB_{prim.}$) – becomes visible and that the annihilation of \bar{p} 's from the secondary interactions is rather small as expected from the schematic Fig. 1. On the other hand, in case of the Au -target the antiprotons from NN channels are annihilated to a large extent especially for $y \leq y_m$ and the surviving \bar{p} 's in the experimental rapidity window $1.0 \leq y \leq 2.0$ [25] practically stem from the secondary production channels. Nevertheless, the experimental data are underestimated on average again by about 30% as in case of the Be -target which might be due to improper elementary cross sections and/or still missing production channels in the transport approach.

The relative antiproton absorption according to Figs. 4–6 strongly depends on rapidity due to a larger formation time τ_F and lower annihilation cross section with increasing rapidity y . In case of $p + Be$ there is practically no \bar{p} annihilation for $y \geq 2$ since the fast antinucleons only form in the vacuum. For the $p + Cu$ system this threshold is shifted to $y \geq 2.6$ while for the $p + Au$ system the annihilation becomes negligible only for $y \geq 3$. The sensitivity to the formation time τ_F is demonstrated in the lower part of the Figs. 5 and 6, where also the final antiproton rapidity spectra are displayed for $\tau_F = 0.4$ fm/c (dashed line) and 1.6 fm/c (dotted line), respectively. In case of the light Be -target no sensitivity to τ_F was found within the numerical statistics of the transport calculations since there is practically no contribution from the mB channels. As can be extracted from Figs. 5 and 6 a

²In Ref. [25] such a feeddown contribution was estimated to be less than 5%.

shorter formation time τ_F leads to an enhancement of the secondary production channel by mB collisions, whereas a larger formation time (~ 1.6 fm/c) essentially suppresses the contribution from secondary meson induced reactions in line with Fig. 1. In fact, the experimental spectra for Cu and Au appear to be better described by $\tau_F = 0.4$ fm/c for the elementary cross sections employed.

The average \bar{p} multiplicity in the rapidity interval $1 \leq y \leq 2$ at 12.3 GeV/c is compared in Fig. 7 as a function of target mass A with the data from [25] for different τ_F . As mentioned before, for the Be -target the calculations for $\tau_F = 0.4, 0.8$ and 1.6 fm/c give approximately the same result, which in comparison to the experimental data is down by about 30% just scratching the lower level of the experimental error bars. For the Cu -target both calculations for $\tau_F = 0.8$ fm/c and $\tau_F = 1.6$ fm/c fall down too low. In case of the Au -target only the calculation for $\tau_F = 1.6$ fm/c is out of range in comparison to the data and also incompatible with the shape of the dN/dy spectra such that a formation time in the order of 1.6 fm/c should be excluded.

We, furthermore, compare our calculations to the system $p + Au$ at 17.5 GeV/c where the E910 Collaboration has taken data, too [25]. In this case (Fig. 8) the most important production channel is due to primary pN inelastic collisions, however, the surviving antiprotons dominantly appear above midrapidity $y_m \approx 1.81$ due to the strong absorption. Within the rapidity window $1 \leq y \leq 2$ of the data the contribution from secondary mB channels is almost compatible (thin solid line, mB_{final} , compared to the dot-dashed line, BB_{final}). The sum of the contributions is reasonably well in line with the experimental data from [25] (lower part) for $\tau_F = 0.8$ fm/c (solid line). A slightly better description is achieved with $\tau_F = 0.4$ fm/c for $y \approx 1-1.5$ in line with the data at 12.3 GeV/c, however, now the \bar{p} rapidity distribution is slightly overestimated for $y \approx 2$. In view of the fact, that the elementary antiproton production cross section is underestimated by about 30% in our calculations, this provides a lower limit for the formation time τ_F .

4 Summary

In this work we have analyzed antiproton production in $p + A$ reactions at AGS energies within the HSD transport approach to examine the apparent low \bar{p} annihilation seen experimentally [25, 46]. Whereas the rather high antibaryon yield in nucleus-nucleus collisions at AGS and SPS energies can be attributed to multi-meson fusion channels employing detailed balance [43, 44, 45] the experimental data in proton-nucleus collisions at AGS energies appear to be compatible with primary proton-nucleon and secondary meson-baryon production channels as also found in Ref. [16] for lower energies.

Detailed calculations employing different hadronic formation times rule out long formation times of the order of 1.6 fm/c (in the hadron rest frame) since such times strongly suppress the meson reinteraction rate. The comparison with the data from the E910 Collaboration instead favors formation times of 0.4-0.8 fm/c when adopting the free antibaryon annihilation cross section. The latter cross section might be

somewhat reduced in the nuclear medium, but it is not likely to be down by factors ~ 5 as quoted in the analysis of Ref. [25]. We have pointed out, furthermore, that especially the high momentum/rapidity part of the \bar{p} spectrum, which dominantly arises from primary pN collisions, shows a sensitivity to the \bar{p} formation time since 'fast' antiprotons may only form in free space and no longer get annihilated in the medium. Unfortunately, this rapidity regime is out of the E910 acceptance such that further experimental studies will be necessary to provide a final answer to the issue of antiproton formation times.

The authors like to acknowledge valuable discussions with C. Greiner.

References

- [1] O. Chamberlain et al., *Nuovo Cimento* 3 (1956) 447.
- [2] T. Elioff et al., *Phys. Rev.* 128 (1962) 869.
- [3] D. Dorfan et al., *Phys. Rev. Lett.* 14 (1965) 995.
- [4] A. A. Baldin et al., *JETP Lett.* 47 (1988) 137.
- [5] J. B. Carroll et al., *Phys. Rev. Lett.* 62 (1989) 1829.
- [6] A. Shor, V. Perez-Mendez, K. Ganezer, *Phys. Rev. Lett.* 63 (1989) 2192.
- [7] W. Cassing, A. Lang, S. Teis, K. Weber, *Nucl. Phys. A* 545 (1992) 123c.
- [8] S. W. Huang, G. Q. Li, T. Maruyama, A. Faessler, *Nucl. Phys. A* 547 (1992) 653.
- [9] P. Danielewicz, *Phys. Rev. C* 42 (1990) 1564.
- [10] E. Hernandez, E. Oset, W. Weise, *Z. Phys. A* 351 (1995) 99.
- [11] J. Schaffner et al., *Z. Phys. A* 341 (1991) 47.
- [12] V. Koch, G. E. Brown, C. M. Ko, *Phys. Lett. B* 265 (1991) 29.
- [13] S. Teis, W. Cassing, T. Maruyama, U. Mosel, *Phys. Rev. C* 50 (1994) 388.
- [14] G. Q. Li, C. M. Ko, X. S. Fang, Y. M. Zheng, *Phys. Rev. C* 49 (1994) 1139.
- [15] C. Spieles, A. Jahns, H. Sorge, H. Stöcker, W. Greiner, *Mod. Phys. Lett. A* 27 (1993) 2547.
- [16] A. Sibirtsev, W. Cassing, G. I. Lykasov, M. V. Rzjanin, *Nucl. Phys. A* 632 (1998) 131.
- [17] W. Cassing, E. L. Bratkovskaya, *Phys. Rep.* 308 (1999) 65.

- [18] C. M. Ko, G. Q. Li, J. Phys. G 22 (1996) 1673.
- [19] C. M. Ko, X. Ge, Phys. Lett. B 205 (1988) 195.
- [20] C. B. Dover, T. Gutsche, M. Maruyama, A. Faessler, Prog. Part. Nucl. Phys. 29 (1992) 87.
- [21] L. Ahle et al., Nucl. Phys. A 610 (1996) 139c.
- [22] J. Barrette et al., Phys. Lett. B 485 (2000) 319.
- [23] B. B. Back et al., Phys. Rev. Lett. 87 (2001) 242301.
- [24] T. A. Armstrong et al., Phys. Rev. C 59 (1999) 2699.
- [25] I. Chemakin et al., Phys. Rev. C 64 (2001) 064908.
- [26] G. I. Veres and the NA49 Collaboration, Nucl. Phys. A 661 (1999) 383c.
- [27] J. Bächler et al., Nucl. Phys. A 661 (1999) 45c.
- [28] F. Antinori et al., Nucl. Phys. A 661 (1999) 130c; R. Caliandro et al., J. Phys. G 25 (1999) 171; F. Antinori et al., Nucl. Phys. A 681 (2001) 165c.
- [29] E. Andersen et al., Phys. Lett. B 449 (1999) 401.
- [30] A. Jahns, H. Stöcker, W. Greiner, H. Sorge, Phys. Rev. Lett. 68 (1992) 2895.
- [31] S. H. Kahana, Y. Pang, T. Schlagel, C. B. Dover, Phys. Rev. C 47 (1993) 1356.
- [32] Y. Pang, D. E. Kahana, S. H. Kahana, H. Crawford, Phys. Rev. Lett. 78 (1997) 3418.
- [33] M. Bleicher et al., Phys. Lett. B 485 (2000) 133.
- [34] H. Sorge, Z. Phys. C 67 (1995) 479; Phys. Rev. C 52 (1995) 3291.
- [35] K. Werner, J. Aichelin, Phys. Lett. B 308 (1993) 372.
- [36] M. A. Braun, C. Pajares, Nucl. Phys. B 390 (1993) 542; N. Armesto, M. A. Braun, E. G. Ferreira, C. Pajares, Phys. Lett. B 344 (1995) 301; M. A. Braun, C. Pajares, J. Ranft, Int. Jour. Mod. Phys. A 14 (1999) 2689.
- [37] N. S. Amelin, N. Armesto, C. Pajares, D. Sousa, Eur. Phys. J. C22 (2001) 149.
- [38] P. Koch, B. Müller, J. Rafelski, Phys. Rep. 142 (1986) 167.
- [39] P. Braun-Munzinger, I. Heppe, J. Stachel, Phys. Lett. B 465 (1999) 15.
- [40] F. Becattini et al., Phys. Rev. C64 (2001) 024901.
- [41] K. Redlich, Nucl. Phys. A 698 (2002) 94c.

- [42] S. Hamieh, K. Redlich, A. Pounsi, Phys. Lett. B 486 (2000) 61.
- [43] R. Rapp, E. Shuryak, Phys. Rev. Lett. 86 (2001) 2980.
- [44] C. Greiner, S. Leupold, J. Phys. G27 (2001) L95.
- [45] W. Cassing, Nucl. Phys. A 700 (2002) 618.
- [46] M. Gonin, O. Hansen, Eur. Phys. J. A7 (2000) 293.
- [47] W. Ehehalt, W. Cassing, Nucl. Phys. A 602 (1996) 449.
- [48] A. Lang, H. Babovsky, W. Cassing, U. Mosel, H.-G. Reusch, K. Weber, J. Comp. Phys. 106 (1993) 391.
- [49] H. Schopper (Editor), Landolt-Börnstein, New Series, Vol. I/12, Springer-Verlag, 1988.
- [50] C. Caso et al., Eur. Phys. J. C 3 (1998) 1.
- [51] J. Geiss, W. Cassing, C. Greiner, Nucl. Phys. A 644 (1998) 107.
- [52] B. Anderson, G. Gustafson, Hong Pi, Z. Phys. C 57 (1993) 485.

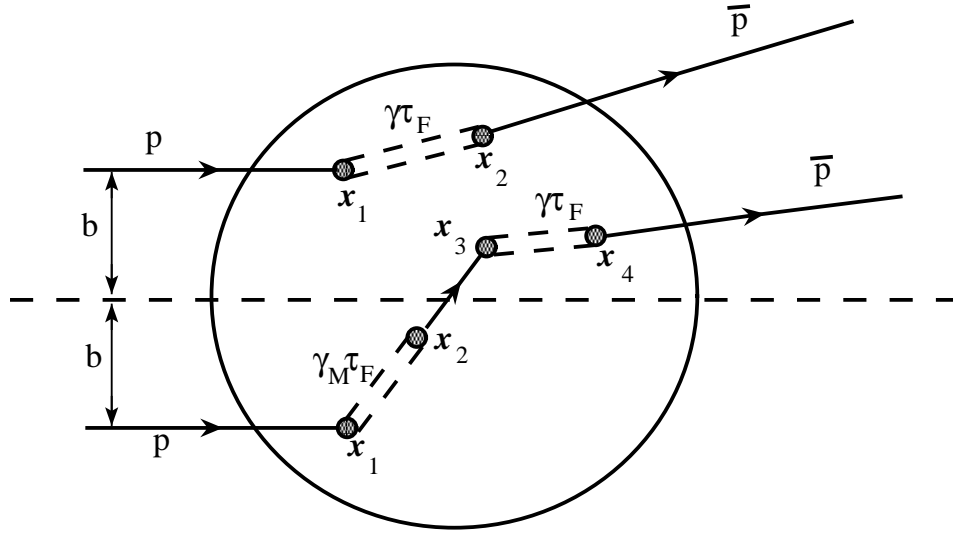


Figure 1: Illustration of primary $p\bar{p}$ production (in x_1), formation (in x_2) and propagation in the nucleus (upper part). The lower part shows the primary production of a pre-meson ($q\bar{q}$ pair) in x_1 , its formation to a hadron in x_2 , the propagation of the hadron in the nucleus and rescattering with another nucleon in x_3 . In the secondary interaction also a pre- $p\bar{p}$ can be created which hadronizes in x_4 and further propagates in the nucleus or in the vacuum (see text).

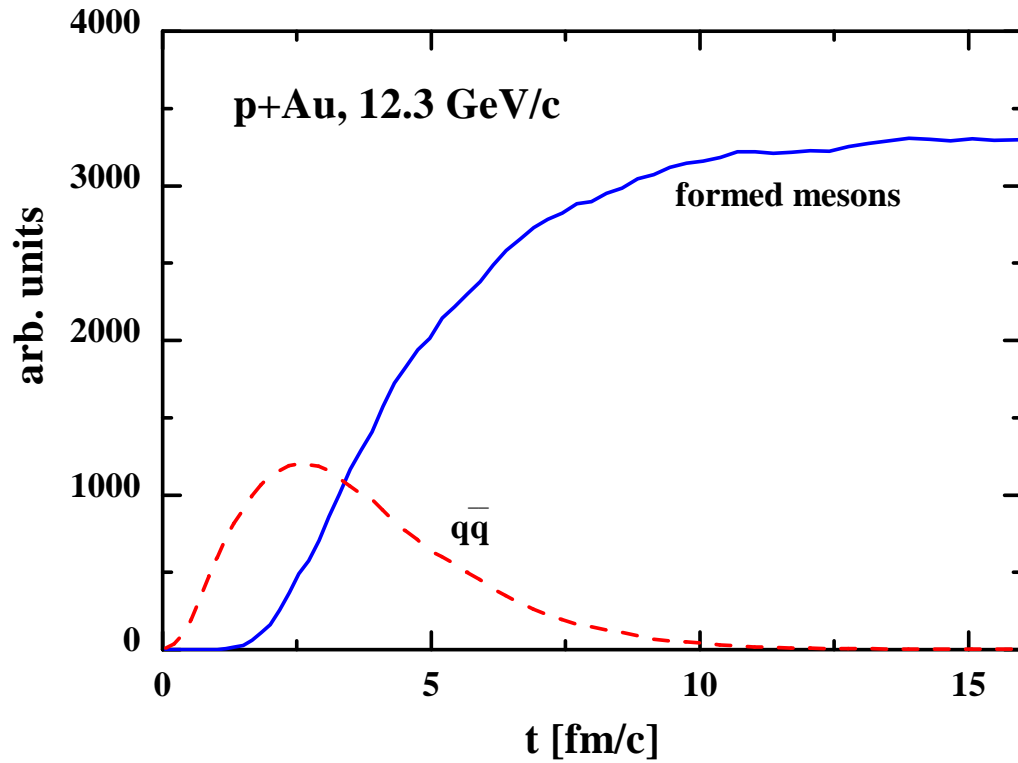


Figure 2: Time evolution of the string-like $q\bar{q}$ excitations (dashed line) and the formed meson number in $p + Au$ reactions at 12.3 GeV/c within the HSD approach employing the 'default' formation time $\tau_F = 0.8$ fm/c. The time is given in the NN center-of-mass system.

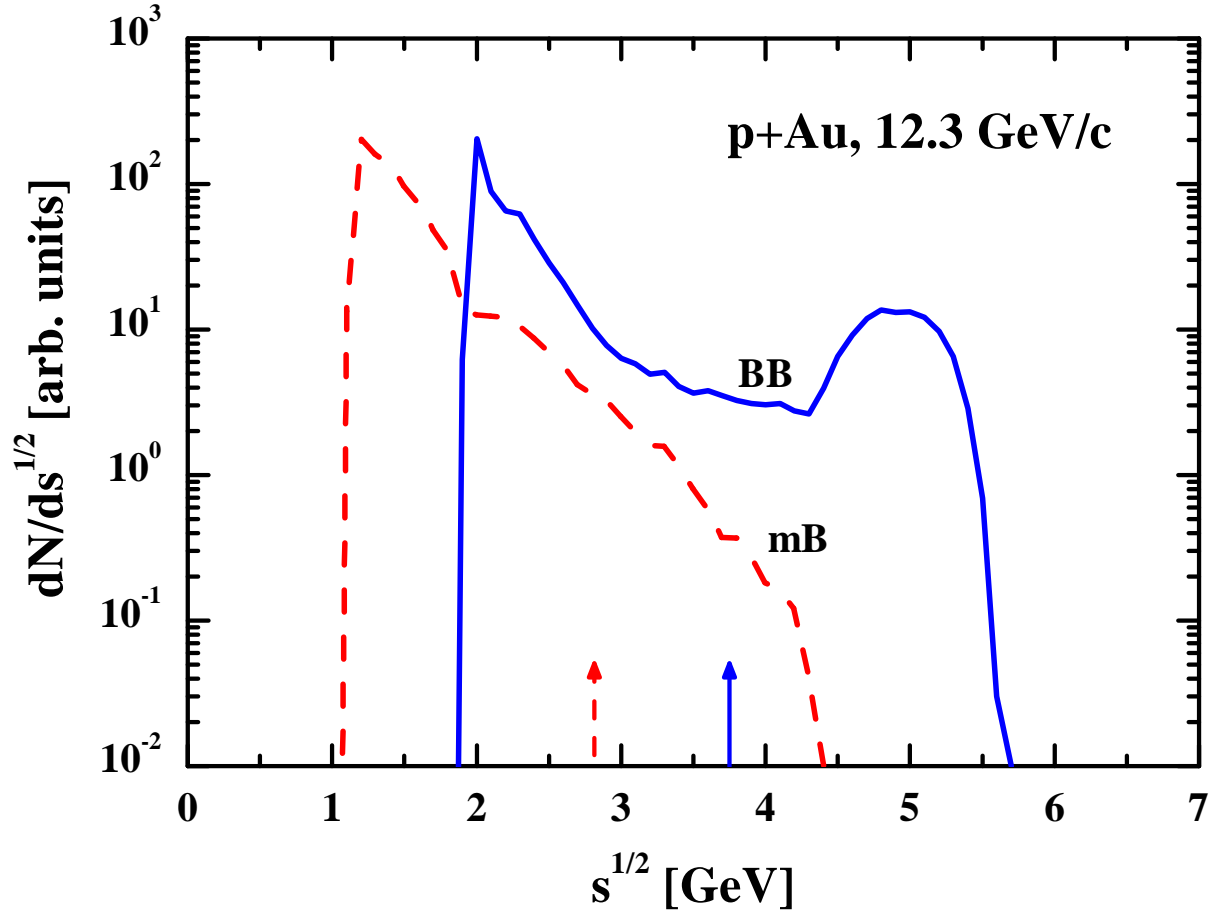


Figure 3: The differential number of baryon-baryon collisions (solid line) and meson-baryon collisions (dashed line) in $p + Au$ reactions at 12.3 GeV/c within the HSD approach employing the 'default' formation time $\tau_F = 0.8$ fm/c. The solid arrow denotes the threshold for $p\bar{p}$ production in BB collisions and the dashed arrow the threshold for mB collisions, respectively.

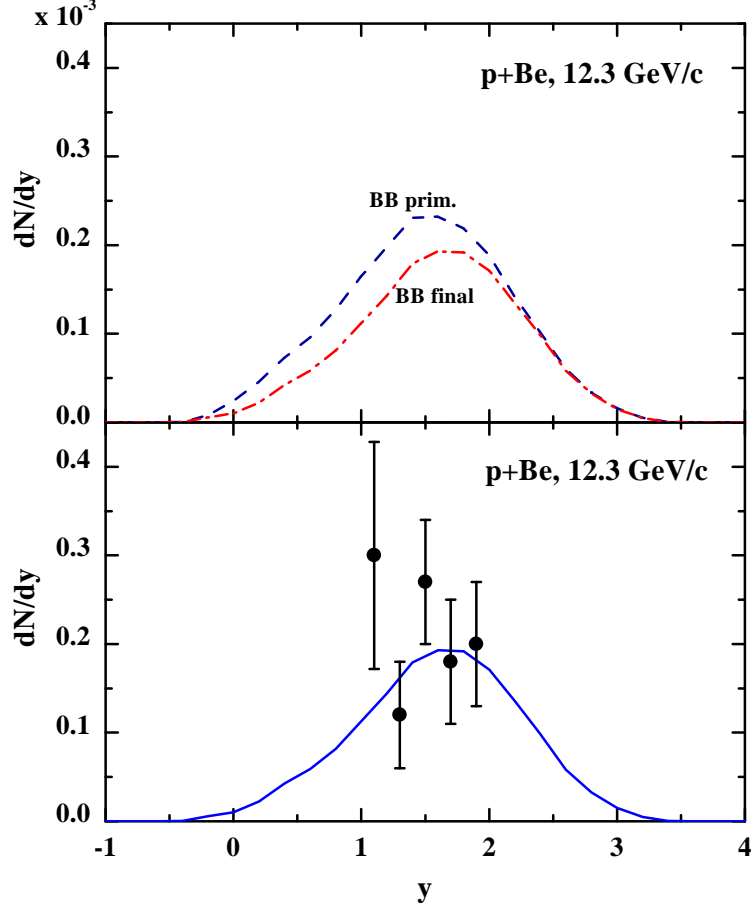


Figure 4: Upper part: Antiproton rapidity distribution in $p + Be$ reactions at 12.3 GeV/c within the HSD approach (dashed line, BB_{prim}) without any final state interactions. The influence of rescattering and \bar{p} annihilation is demonstrated in comparison to the dash-dotted line (BB_{final}), which shows the final antiproton rapidity distribution. Note that there is no longer \bar{p} annihilation for $y \geq 2$ for the formation time $\tau_F = 0.8$ fm/c adopted in the calculations. The contribution from mB channels to antiproton production in this system is not visible on a linear scale. Lower part: Comparison of the calculated \bar{p} rapidity distribution (for $\tau_F = 0.8$ fm/c) with the experimental data from Ref. [25]. Within the statistics achieved in the transport calculations there is no change in the \bar{p} rapidity distribution when changing τ_F in the interval [0.4, 1.6] fm/c.

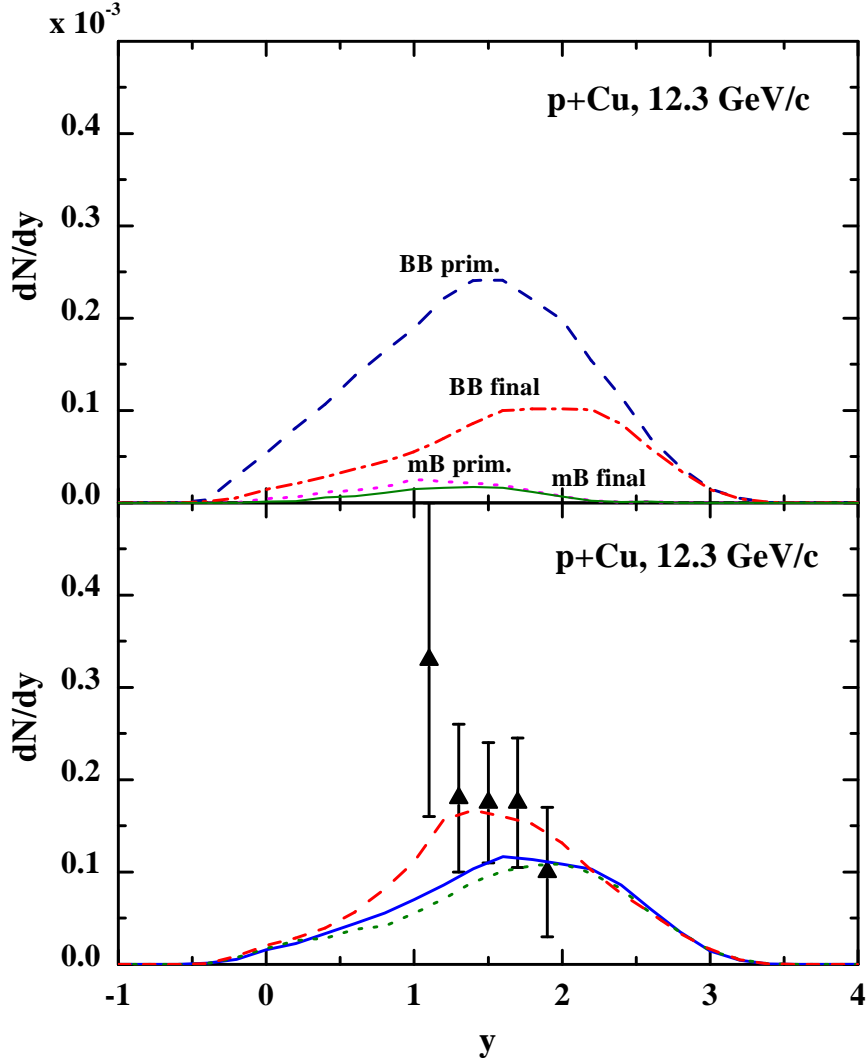


Figure 5: Upper part: Antiproton rapidity distribution in $p + Cu$ reactions at 12.3 GeV/c within the HSD approach for baryon-baryon production channels (dashed line, BB_{prim}) without any final state interactions. The influence of rescattering and \bar{p} annihilation is demonstrated in comparison to the dash-dotted line (BB_{final}), which shows the final antiproton rapidity distribution from BB channels for a formation time $\tau_F = 0.8$ fm/c. The short dashed line displays the contribution from secondary meson-baryon (mB) reactions without FSI while the thin solid line corresponds to the final \bar{p} rapidity distribution from mB reactions including rescattering and annihilation. Lower part: Comparison of the calculated final \bar{p} rapidity distribution from BB and mB collisions (solid line for $\tau_F = 0.8$ fm/c) with the experimental data from Ref. [25]. The dashed and dotted lines demonstrate the results for $\tau_F = 0.4$ fm/c and 1.6 fm/c, respectively.

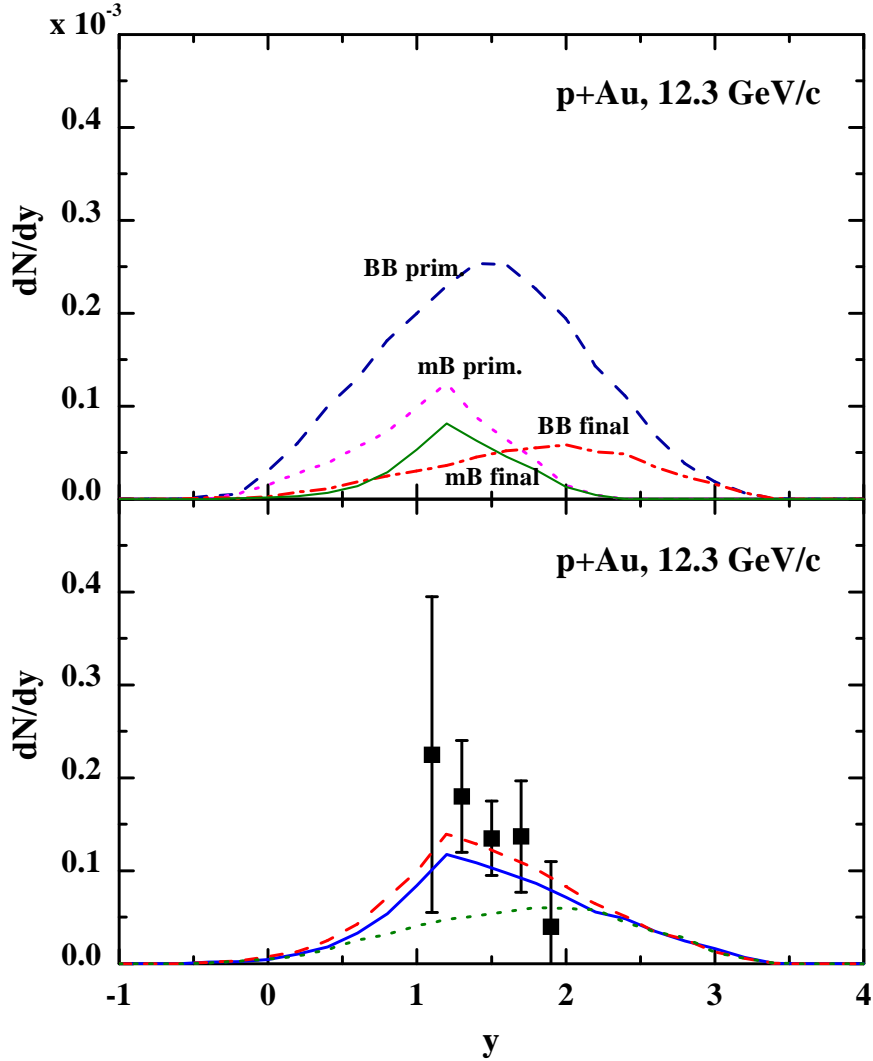


Figure 6: Upper part: Antiproton rapidity distribution in $p + Au$ reactions at 12.3 GeV/c within the HSD approach for baryon-baryon production channels (dashed line, BB_{prim}) without any final state interactions. The influence of rescattering and \bar{p} annihilation is demonstrated in comparison to the dash-dotted line (BB_{final}), which shows the final antiproton rapidity distribution from BB channels for a formation time $\tau_F = 0.8$ fm/c. The short dashed line displays the contribution from secondary meson-baryon (mB) reactions without FSI while the thin solid line corresponds to the final \bar{p} rapidity distribution from mB reactions including rescattering and annihilation. Lower part: Comparison of the calculated final \bar{p} rapidity distribution from BB and mB collisions (solid line for $\tau_F = 0.8$ fm/c) with the experimental data from Ref. [25]. The dashed and dotted lines demonstrate the results for $\tau_F = 0.4$ fm/c and 1.6 fm/c, respectively.

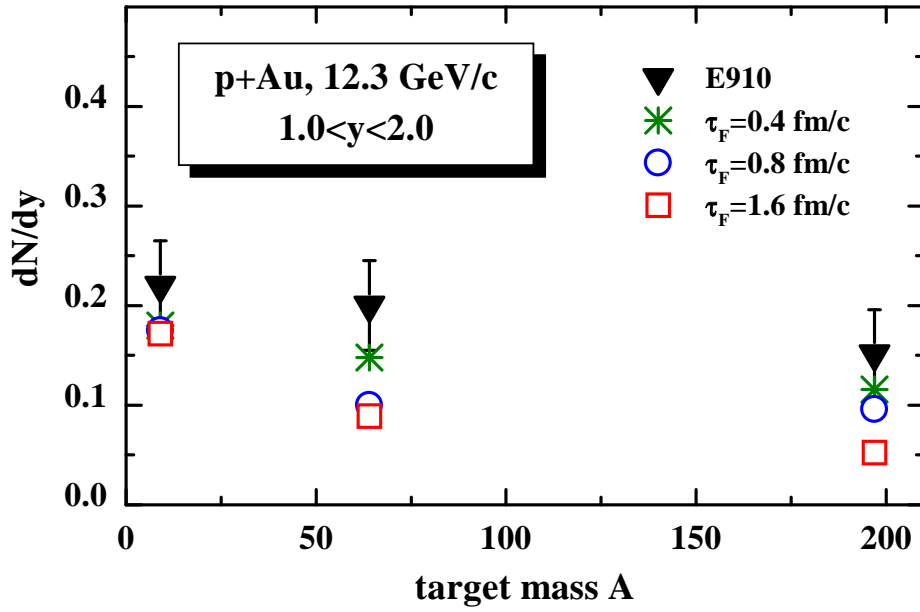


Figure 7: Antiproton rapidity distribution in $p + A$ reactions at $12.3 \text{ GeV}/c$ within the HSD approach for different formation times $\tau_F = 0.4, 0.8$ and $1.6 \text{ fm}/c$ for Be , Cu and Au targets. The experimental data (full triangles) have been adopted from Ref. [25].

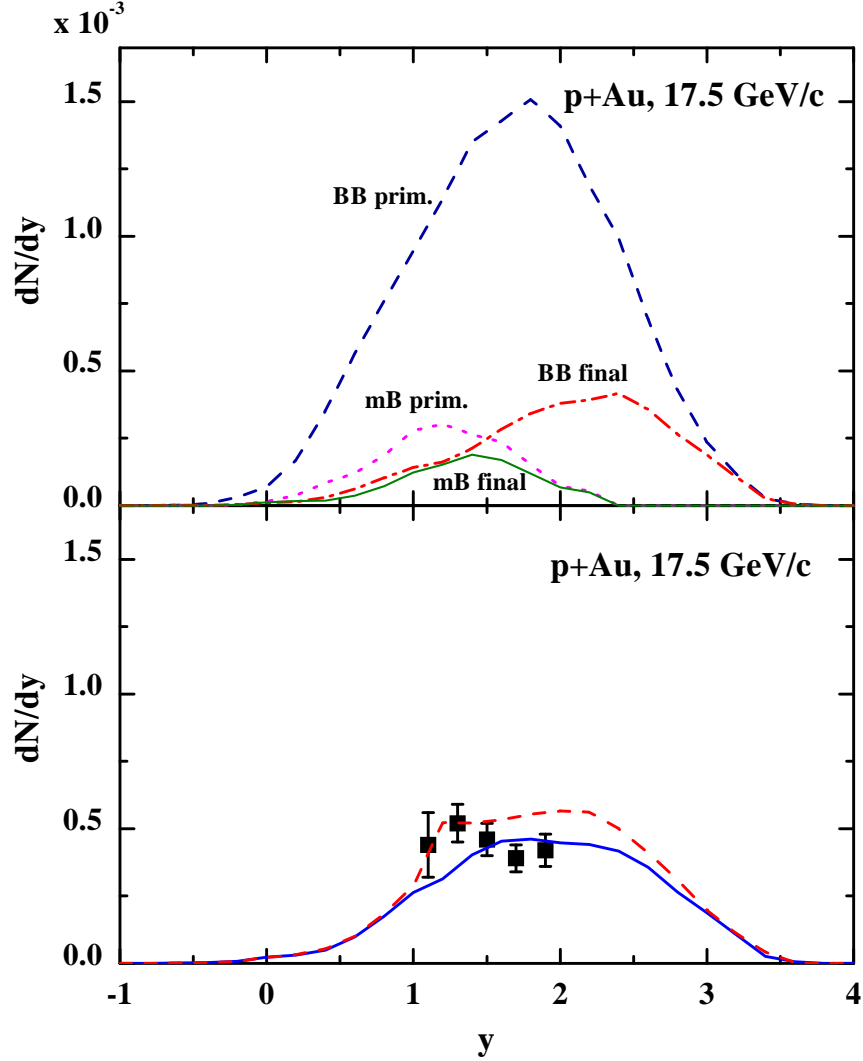


Figure 8: Upper part: Antiproton rapidity distribution in $p + Au$ reactions at 17.5 GeV/c within the HSD approach for baryon-baryon production channels (dashed line, BB_{prim}) without any final state interactions. The influence of rescattering and \bar{p} annihilation is demonstrated in comparison to the dash-dotted line (BB_{final}), which shows the final antiproton rapidity distribution from BB channels for a formation time $\tau_F = 0.8$ fm/c. The short dashed line displays the contribution from secondary meson-baryon (mB) reactions without FSI while the thin solid line corresponds to the final \bar{p} rapidity distribution from mB reactions including rescattering and annihilation. Lower part: Comparison of the calculated final \bar{p} rapidity distribution from BB and mB collisions (solid line: $\tau_F = 0.8$ fm/c; dashed line: $\tau_F = 0.4$ fm/c) with the experimental data from Ref. [25].